CHAPTER – 4

Phase Evolution, Thermal Stability and Indentation Behavior of MgAlSiCrFeNi Low-Density High Entropy Alloy Processed through Mechanical Alloying and Spark Plasma Sintering

CHAPTER 4

PHASE EVOLUTION, THERMAL STABILITY AND INDENTATION BEHAVIOR OF MgAlSiCrFeNi LOW-DENSITY HIGH ENTROPY ALLOY PROCESSED THROUGH MECHANICAL ALLOYING AND SPAK PLASMA SINTERING

This Chapter consists of detailed synthesis and characterization of equiatomic MgAlSiCrFeNi low density high-entropy alloy (HEA) through mechanical alloying (MA) followed by spark plasma sintering (SPS). Nickel (Ni) was added in equiatomic proportion in previously studied MgAlSiCrFeNi HEA to understand the overall effect on the alloy behaviour. The alloying behavior, phase evolution, phase composition and thermal stability of as-milled nanostructured powders and sintered compacts of HEA were ascertained through X-ray diffraction (XRD) and transmission electron microscopy (TEM), scanning electron microscopy (SEM) and differential scanning calorimetry (DSC), respectively. The positive mixing enthalpy between Mg and most of the other elements may not favor solid solution formation. Hence, powder metallurgy processing route, MA and SPS were adopted to synthesize this LDHEA. Various thermodynamics parameters were calculated in order to correlate the experimental findings of phase evolution and stability of the annealed powder and spark plasma sintered alloy.

4.1 XRD analysis of MgAlSiCrFeNi high entropy alloy

The diffraction patterns of mechanical alloyed MgAlSiCrFeNi HEA powders, milled up to 60h are displayed in figure 4.1. Initially, at 1 h, diffraction peaks corresponding to all the constituent elements i.e., Mg (hP2; a=0.3209 nm, c=0.5211 nm), Al (cF4; a=0.4049 nm), Si (cF8; a=0.5430 nm), Cr (cI2; a=0.2884 nm), Fe (cI2; a=0.2866 nm), and Ni (cF4; a=0.3524 nm) are identified in the diffraction pattern. After 10 h of MM, the peak intensity of all constituent elements started decreasing. It has been noticed that the elements of low melting point, i.e., Mg and Al have started disappearing. Moreover, peaks corresponding to Mg along with weak peaks of Al are not observed after 10 h of MM. At

20 h of MM, all major peaks related to Al have completely disappeared; however, peaks corresponding to Si, Cr, Fe, and Ni (only at d~0.2034 nm, 0.1762 nm) are evident.

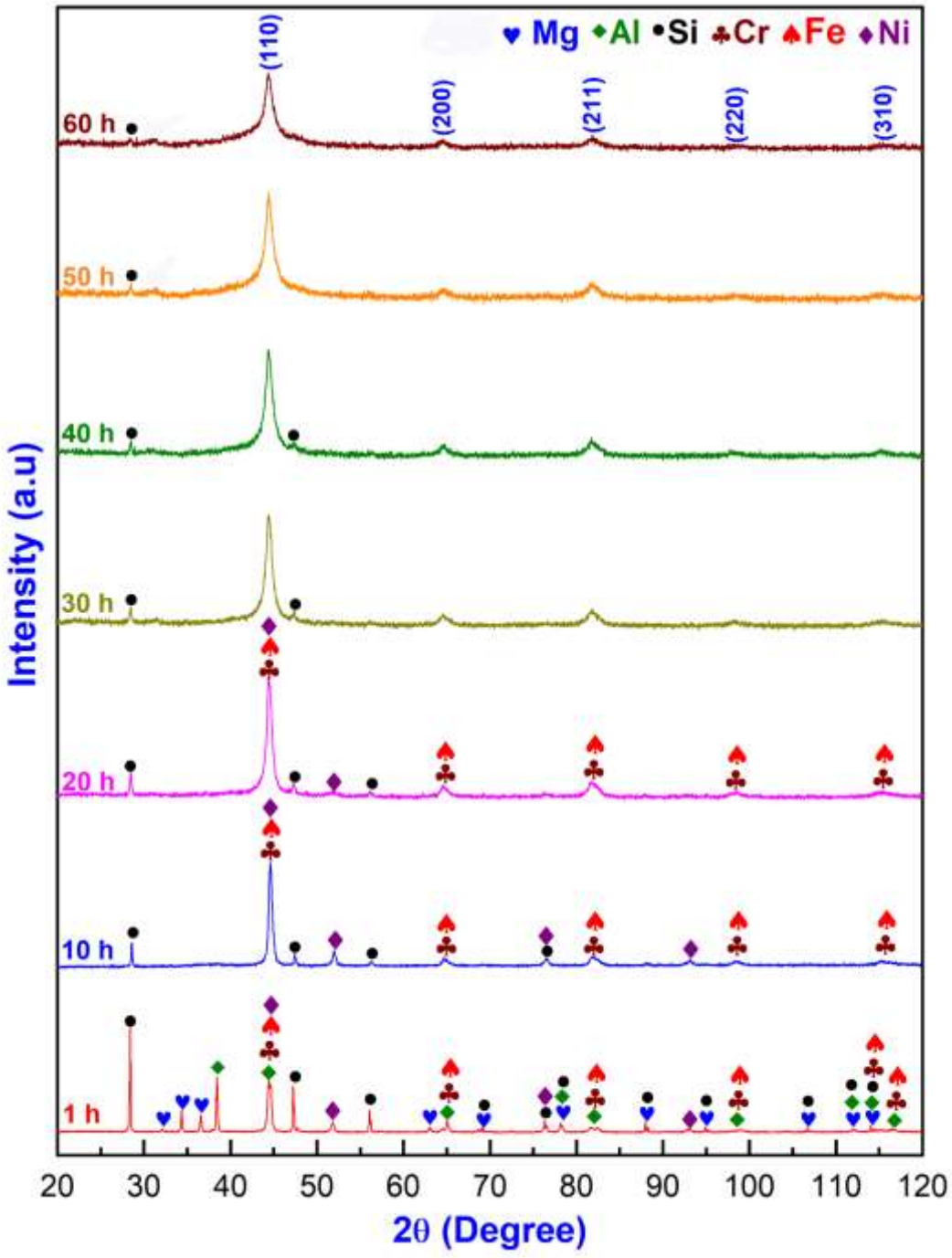

Figure 4.1: Phase evolution during mechanical alloying of MgAlSiCrFeNi HEA powder upto 60 h.

The presence of Cr and Fe may be discerned from the assymmetricity of the peak corresponding to (110) reflection of Fe (d~0.2027 nm). After 30 h of milling, a BCC phase along with a minor amount of Si can be discerned. The presence of BCC phase was confirmed by indexing of the planes i.e., (110), (200), (211), (220), and (310) structure. Only first two intense reflections of Si such as (111) (d~0.3138 nm), and (220) (d~0.1920 nm) were observed. Although, the 30 h of milling is sufficient for the formation of the major BCC, however, to incorporate the whole amount of Si into the BCC phase, the milling was continued till 60 h. The reduced intensity of intense reflection of Si, i.e., (111) & (220), were observed till 40 h of milling indicates decrease in the amount of undissolved Si.

Table 4.1. Variation of crystallite size (nm), lattice strain (%) and dislocation density along with milling time for MgAlSiCrFeNi HEA.

Milling Duration (h)	**Crystallite size (nm)**	**Lattice strain (%)**	**Dislocation density (m^{-2})**
1h	-	-	-
10 h	18	0.52	0.892×10^{18}
20 h	13	0.76	1.82×10^{18}
30h	11	0.90	2.65×10^{18}
40 h	9	1.02	3.46×10^{18}
50 h	9	1.07	3.72×10^{18}
60 h	8	1.15	4.38×10^{18}

Further milling of the powder till 60 h led to the significant broadening in the diffraction peaks. The broadening of the peaks indicates the nanostructuring and induction of lattice strain in powder. The systematic variation of crystallite size, lattice strain and dislocation density was followed with milling duration (Table 4.1). It could be noticed that the crystallite size decreases and lattice strain increases with milling. Refinement of

crystallite size from the order of ~18 nm (10 h) to ~ 8 nm and increase in lattice strain (%) from 0.52 to 1.15 was observed after 60 h of milling. The increase in lattice strain is due to the mechanical deformation caused during the milling by the increased dislocation density. The dislocation density was evaluated as described in Chapter 2 and the dislocation density was found to lie from 0.892 x 10^{18} m^{-2} (10 h of MM) to 4.38 x 10^{18} m^{-2} (60 h of MM).

4.2 Nanostructured nature and powder morphology of milled powder

The structural evolution and fine microstructural characteristics were examined under TEM (Figure 4.2). The micrographs showing bright field images (a, d) and selected area diffraction patterns (SADPs) (b, e), and dark field images (c, f) of 60 h MM powder reveals the presence of a BCC phase coexisting with the minor amount of undissolve Si. The bright-field image (Figure 4.2(a)) reveals the heavy deformation induced during the MA and can be observed in the powder particle. The grains of ≤ 20 nm were also identified in the milled powder particles. This observation agrees well with the results of XRD experiment of 60 h MM powder revealing considerable peak broadening. Figure 4.2 (b), revealed the polycrystalline nature of the alloy by forming the ring pattern corresponding to the BCC phase. These rings are indexed as (110), (200), and (211) planes of BCC phase. Figure 4.2 (c) shows dark field image collected from the (110) plane, which confirms the nanocrystalline nature of the milled powder of sizes ~15±4 nm. These results match closely to that of the crystallite size obtained from XRD (Figure 4.1). Figure 4.2 (d) shows the presence of flaky particles along with the dark patches.

The existence of dark flaky particles in bright field image is mainly due to the diffraction contrast and thickness effect. However, the variation in the thickness of the particles develops the amplitude contrast because the electron beams interact with the more material. Retained Si in the alloy powder may create the variation of thickness which

appears dark in nature. The presence of undissolved Si along with the parent BCC phase may be discerned from the SADP shown in Figure 4.2 (e).

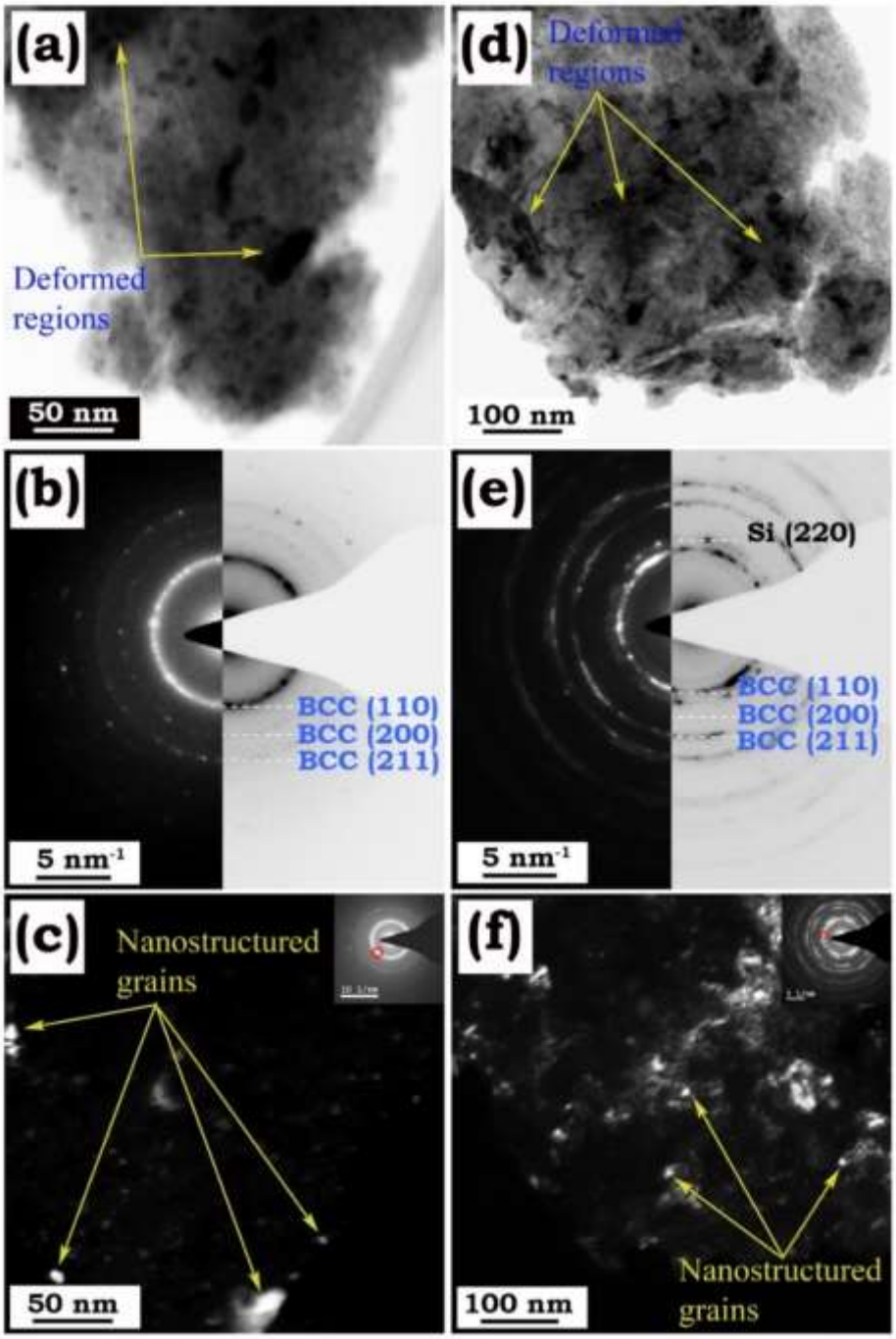

Figure 4.2: TEM micrograph showing (a, d) bright field image and (b, e) selected area diffraction pattern and (c. f) dark field image of LDHEA powder milled for 60 h showing presence of BCC along with minor fraction of Si.

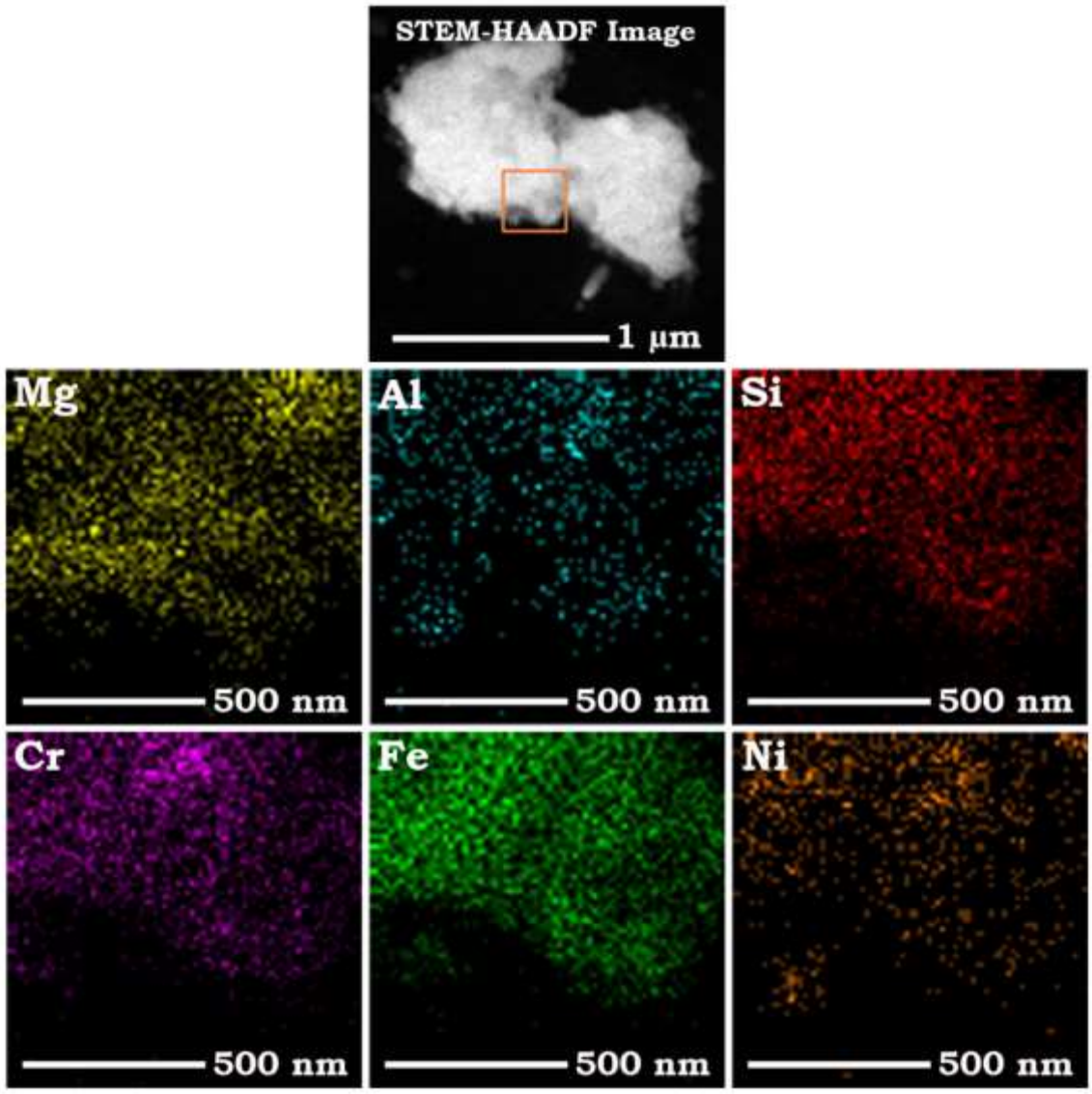

Figure 4.3: STEM-EDS mapping of equiatomic MgAlSiCrFeNi high entropy alloy mechanically alloyed for 60h showing elemental distribution

The (220) reflection of Si is marked along with the polycrystalline rings which correspond to that of the BCC phase. This confirms the findings of a minor amount of retained Si along with a BCC phase in milled powder.

The STEM-EDS elemental mapping of 60 h milled powder is given in Figure 4.3. The presence of homogeneous distribution of all the elements could be observed with slight variation in the intensity of element like Ni. The variation in the intensity of Ni may be

attributed to non-uniform thickness of powder particles examined in the present study. The incorporation of the elements into a BCC lattice identified by XRD and TEM results was confirmed.

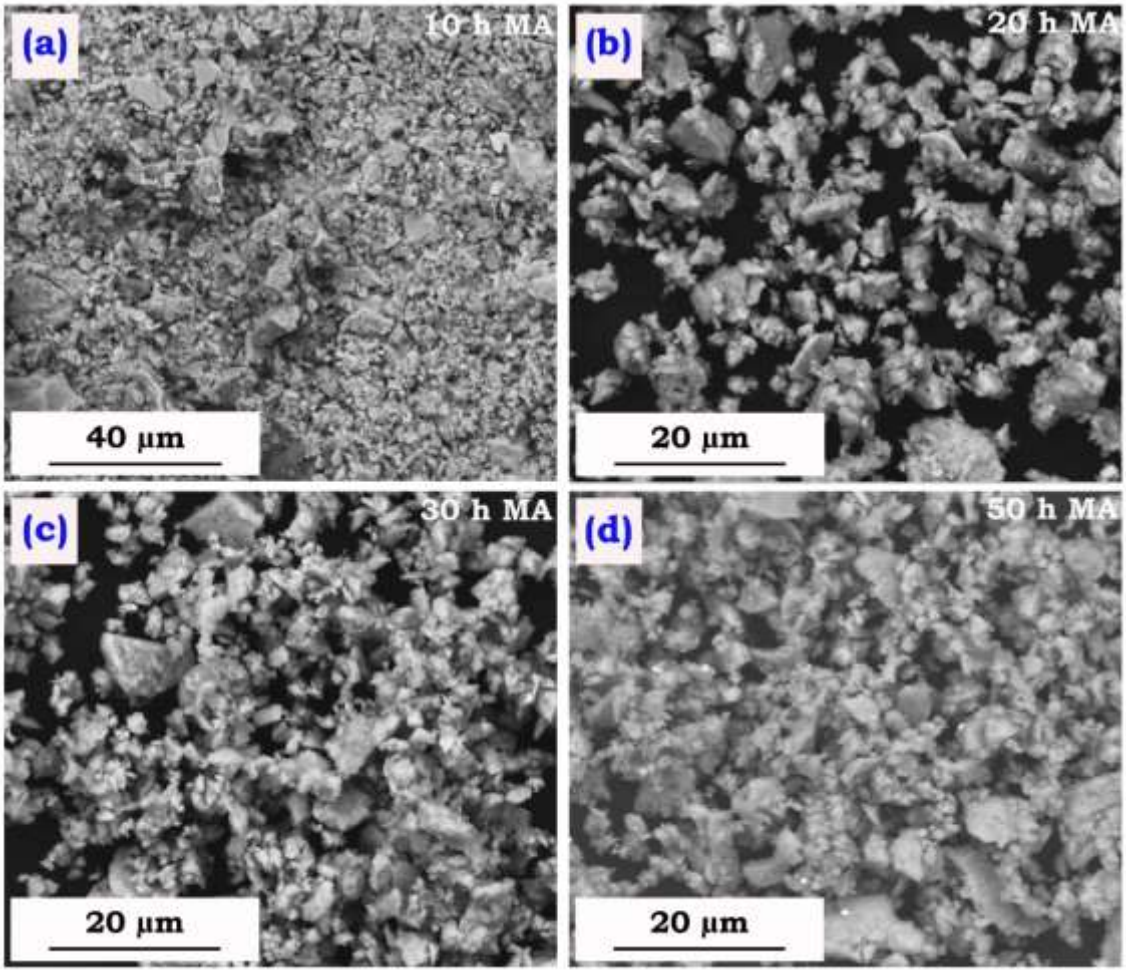

Figure 4.4: Morphology of MgAlSiCrFeNi HEA powder mechanically milled for (a) 10 h; (b) 20 h; (c) 30 h; (d) 50 h.

Figure 4.3 shows that the Si is also uniformly distributed in the investigated particle, thereby establishing the fact that only a very small amount of Si could not be dissolved even after 60 h of milling.

Table 4.2: Elemental compsoition of MgAlSiCrFeNi milled HEA powder for 60 h.

		Mg	**Al**	**Si**	**Cr**	**Fe**	**Ni**
Intial composition	0 h	16.66	16.66	16.66	16.66	16.66	16.66
Final composition	60 h	18.11	18.54	16.96	14.24	14.76	17.39

The BSE-SEM micrographs of Figure 4.4 (a), (b), (c), and (d) show the morphology of milled powder for 10 h, 20 h, 30 h and 50 h respectively. It is shown from Figure 4 about irregularity in shape and size. Figure 4.4 (a) & (b) represents non-uniform color contrast for 10 h and 20 h milled powders. On increasing the duration of milling to 30 h, the non-uniformity in the contrast has almost disappeared, which can be attributed to uniform distribution of the elements. Further milling till 60 h, it only confirms to the homogenous distribution of the elements. The non-uniformity in the color contrast is due to the dependence of contrast on the alloying elements' atomic number. The homogeneity in comparison is, therefore, the evidence of the formation of alloy with homogenous alloying. This was already observed with XRD, TEM, and STEM-EDS images. The final elemental composition of milled powder is reported in Table 4.2 and shows the final composition almost closer to the initial composition.

4.3 Thermal stability of the milled powder

The thermal stability of the milled powder was studied through DSC by heating the powder up to 1200 ℃ (1473 K) is given in figure 4.5. The thermal profile shows five exothermic events indicated as T1, T2, T3, T4, and T5 at temperature of 424 ℃ (697 K), 550 ℃ (823 K), 669 ℃ (942 K), 874 ℃ (1147 K), and 958 ℃ (1231 K) respectively. In

order to further assure the dynamics of phase evolution at particular heat events as observed in DSC, the powder samples were annealed upto 800 ℃ (1073 K).

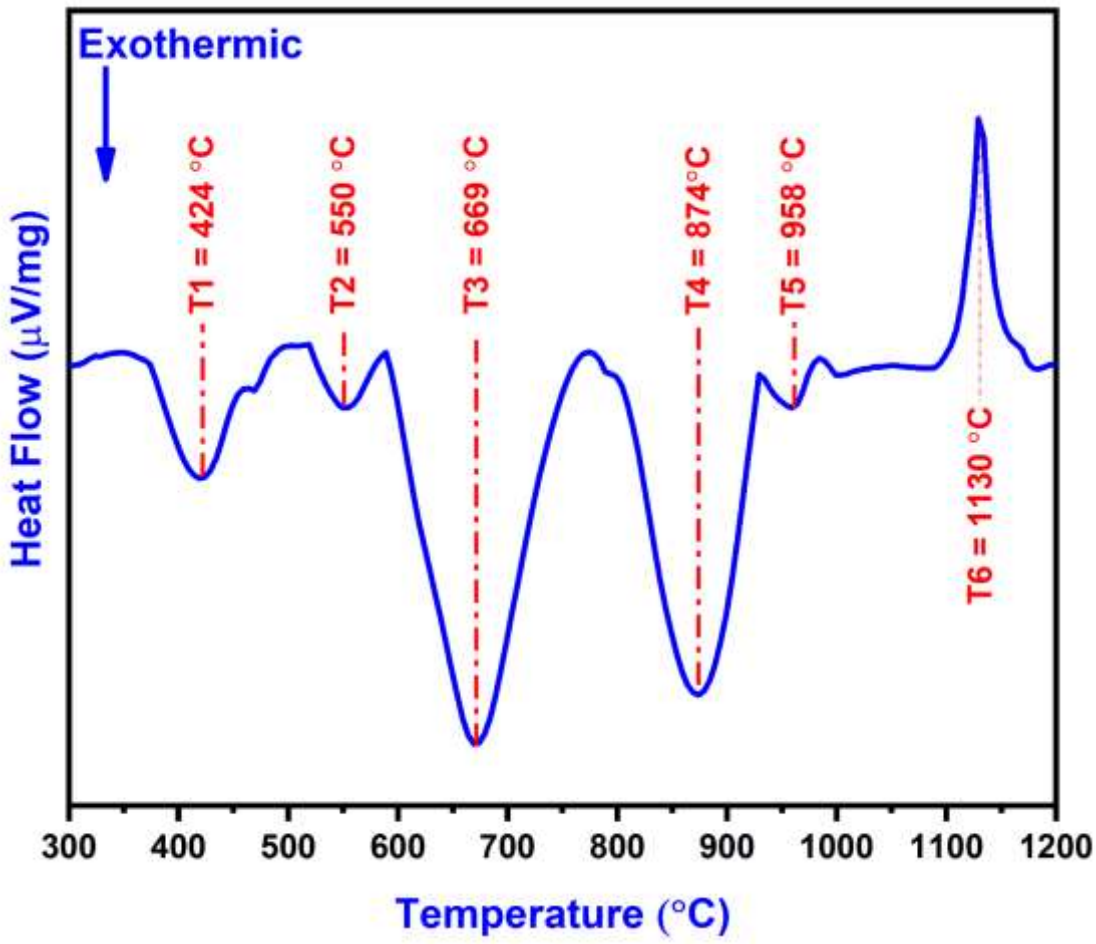

Figure 4.5: DSC thermogram of MgAlSiCrFeNi HEA powder milled for 60 h showing exothermic and endothermic heating events.

The diffraction patterns of HEA powder at room temperature, and during annealing at 400 ℃ (673 K), 500 ℃ (773 K), 600 ℃ (873 K), 700 ℃ (973 K), and 800 ℃ (1073 K) are shown in Figure 4.6. The 60 h milled powder contains a BCC phase as major one along with a minor one as the undissolved Si. No sign of any additional phases was observed up to 400 ℃ (673 K), as depicted from Figure 4.6 (a). It confirms that the alloy is thermally stable upto 400 ℃ (673 K). Some differences in the results can be present while comparing

the thermal stability of the non-isothermal heat-treatment in DSC and isothermal annealing treatment. In the present investigation, it is challenging to affirm the type of B2 phase formed during annealing. On annealing the powder at 500 ℃ (773 K), additional peaks corresponding to the partially ordered B2 type phase (a=0.2889 nm; PDF card No.: 65-6132) and minor amount of FCC Al-Mg solid solution phase (a=0.4082 nm; PDF card no.: 01-077-6796) designated as FCC1 was evident. The existence of partially ordered B2-type phase was established presence of the superlattice refection such as (100) (at 2θ=31.02º) as shown in Figure 4.6 (a). Annealing treatment at 600 °C (873 K) leads to formation of monoclinic $Al_{13}Fe4$ (a=1.549 nm, b=0.808 nm, c=1.248 nm; PDF card no.: 01-073-3008), Mg_2Si (a=0.6351 nm; PDF card no.: 00-034-0458) in addition to the parent BCC and B2 phase. Further annealing at 700 °C, the formation of another Al-Mg solid solution referred to as FCC 2 (cF4; 0.4215 nm; PDF card no.: 01-077-6799) and Cr_5Si_3 (tI32; a=0.9165 nm, c=0.4638 nm; PDF card no.: 00-051-1357) along with $Al_{13}Fe_4$, Mg_2Si phase, with BCC and B2 phase were observed. Annealing at 800 °C (1073 K), almost similar phases were observed except FCC1 and Mg_2Si phases. The Figure 4.7 represents TEM micrograph of MgAlSiCrFeNi LDHEA powder annealed at 800 ℃ (1073 K) for 60 min. It can be discerned from the bright field image of annealed LDHEA powder that nano-precipitates are formed inside the BCC matrix of LDHEA as marked in the Figure 4.7 (a). The SAD pattern of the annealed LDHEA powder particle investigated in the present study shows the presence of BCC phase along with B2-type and $Al_{13}Fe_4$ phase (Figure 4.7 (b)). Further, it represents the electron diffraction spot corresponding to (100) reflection of B2-type phase. The existence of (100) spot ascertains the evolution of the B2-type phase after annealing of the LDHEA powder. This is in line with the findings of the XRD as observed in the Figure 4.6 (a).

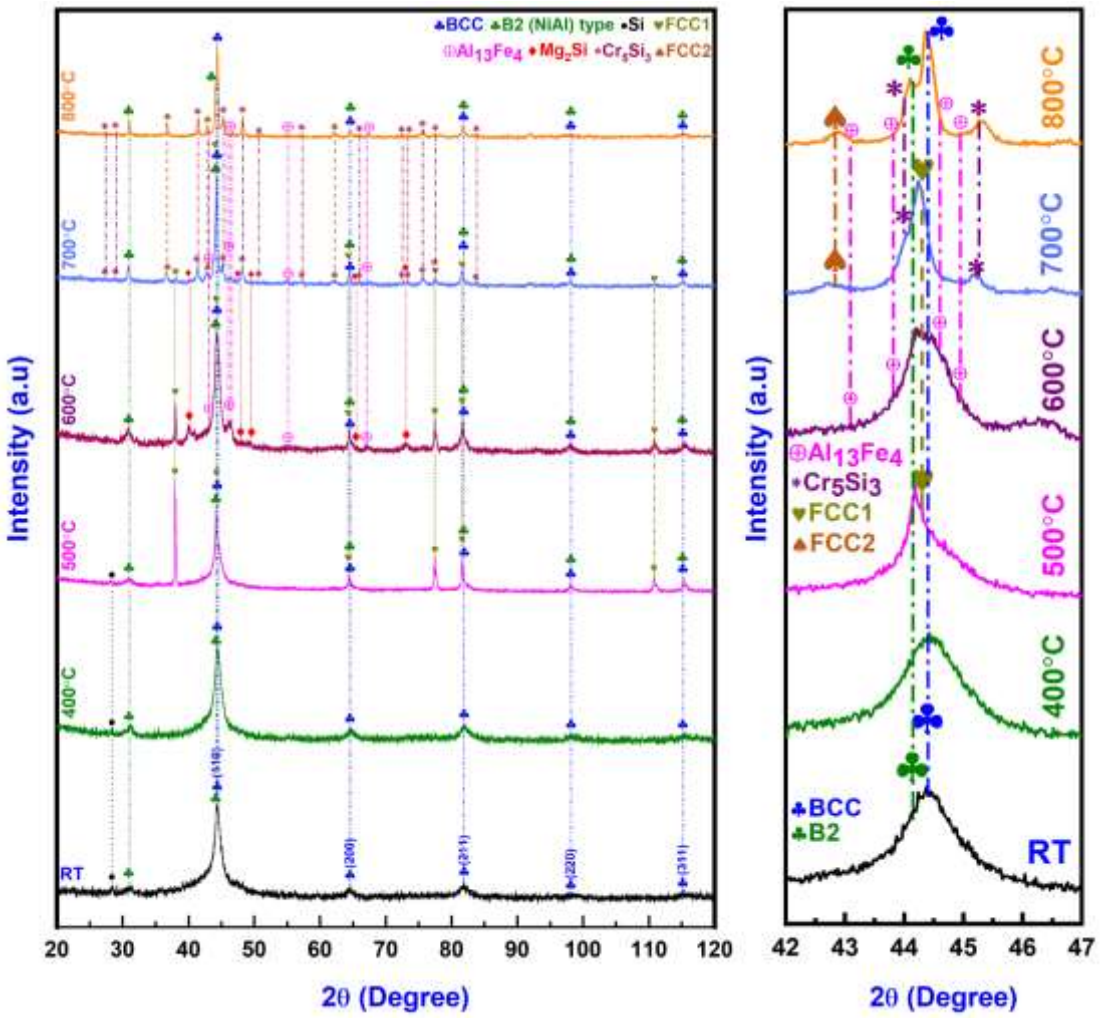

Figure 4.6: (a) Phase evolution during annealing of 60 h milled MgAlSiCrFe HEA powder upto 800 °C (1073K); (b) blown-up image for (110) peak of BCC phase showing evolution of other phases.

The dark field image of annealed powder shown in the Figure 4.7 (c) represents the existence of nanostructured grains and nano-precipitates corresponding to the (110) plane of B2-type and parent BCC phase. The nanostructured grains in the annealed powder samples are marked by arrows in the Figure 4.7 (c).

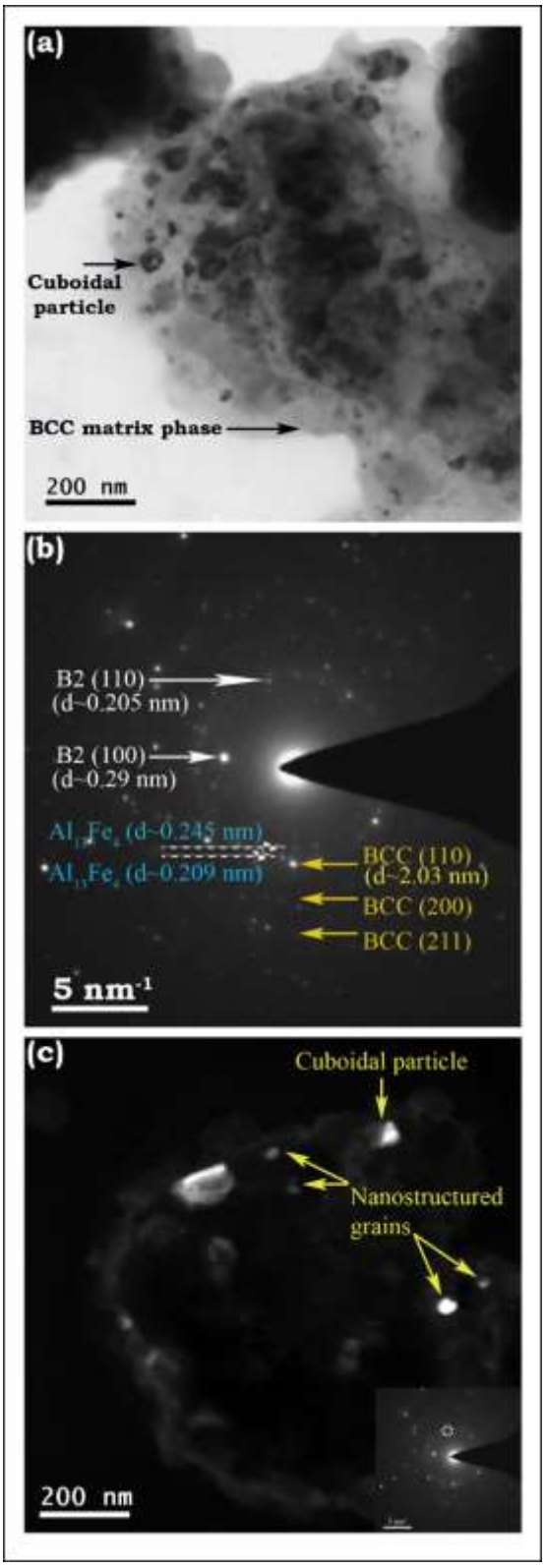

Figure 4.7: TEM micrograph showing (a) bright field image and (b) selected area diffraction patterns and (c) dark field images of MgAlSiCrFeNi LDHEA annealed powder at 800 ℃ (1073K) for 60 min.

4.4 Consolidation and microstructural evolution of MgAlSiCrFeNi HEA

Figure 4.8 has shown phases evolved in 60 h milled LDHEA powder consolidated at 800 ℃ (1073 K) for 15 min through spark plasma sintering. The parent BCC phase was able to retain with identity along with the B2 type phase. Apart from these two major phases, a minor amount of intermetallics and silicides were also observed. The minor amount of FCC2, $Al_{13}Fe_4$, and Cr_5Si_3 formed after SPS is marked in Figure 4.8 (a). These are also in line with the phases observed in the 800 ℃ (1073 K) annealed sample. The (110) peak of the BCC phase was exploded to show the minor phases illustrated in Figure 4.8 (b). The intense peak of Cr_5Si_3 [i.e, (202)(d~0.2069 nm), (411)(d~0.2069) and (222)(d~0.1886 nm)] and $Al_{13}Fe_4$ [i.e, (620)(d~0.2101 nm), (332)(d~0.2094) and (025)(d~0.2048 nm)] and other minor phases are systematically marked in Figure 4.8 (b). The (110) peak of the major BCC phase was deconvoluted, as shown in Figure 4.8 (c).

The deconvoluted peaks represent the (110) peak of BCC and B2 phases at d~0.2038 nm and d~0.2058 nm, respectively. The goodness of fit for (110) peak of BCC and B2 phase was ≥95%, while the minor phases are not significant fraction as their goodness of fit was not good. Figure 4.9 represents the BSE-SEM micrograph of the SPSed sample of LDHEA at 800 ℃ for 15 min. The distribution of grains with various shapes and sizes can be discerned from Figures 4.9 (a & b) at different magnification and its elemental composition (Table 4.3). The sintered sample does not have any significant evidence of porosity, as determined in Figure 9 and evident from the relative density of SPSed LDHEA sample mentioned in Table 4.4. A few pores observed in the microstructure of the sintered samples are marked with the help of arrows as shown in the Figure 4.9 (b).

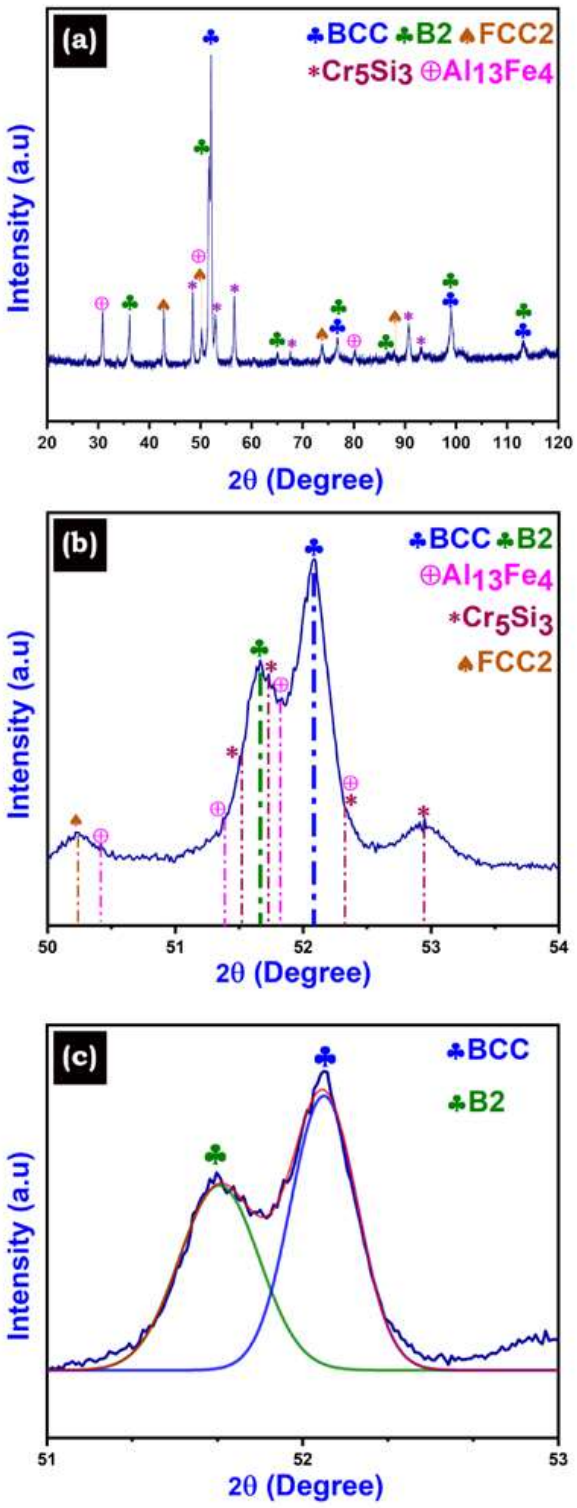

Figure 4.8: Phase formation in MgAlSiCrFeNi HEA powder spark plasma sintered at 800 ℃ (1073K) for 15 min (a); Blown-up image showing BCC/B2 phase along with other minor phases (b); Deconvoluted peak showing the presence of BCC and B2 phase after SPS.

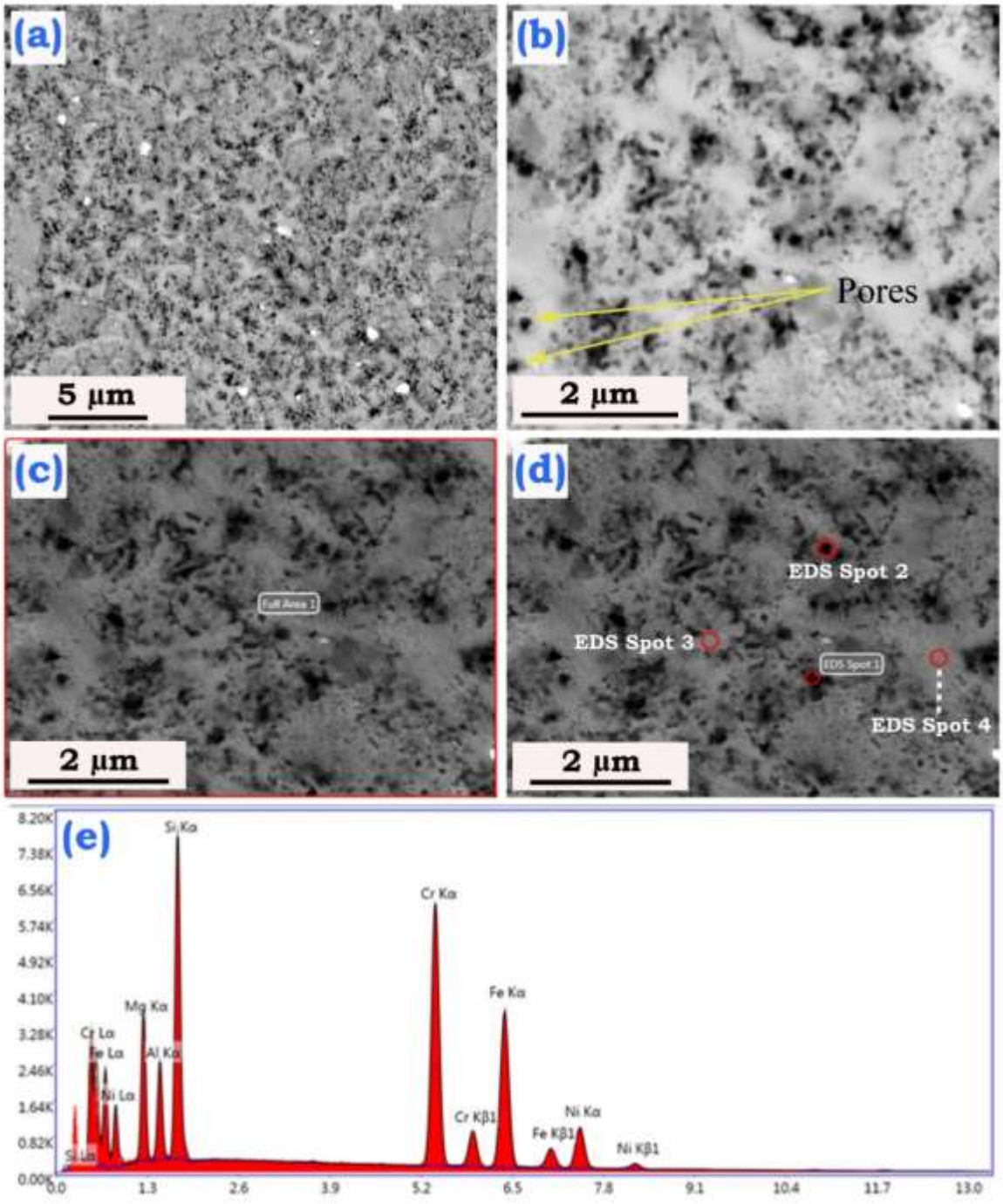

Figure 4.9: Back-scattered SEM micrograph showing coarse and fine microstructure of spark plasma sintered MgAlSiCrFeNi HEA in (a) and (b) respectively. (c) and (d) shows the area and points for area and point EDS analysis respectively. (e) EDS spectrum corresponding to the full area scanning.

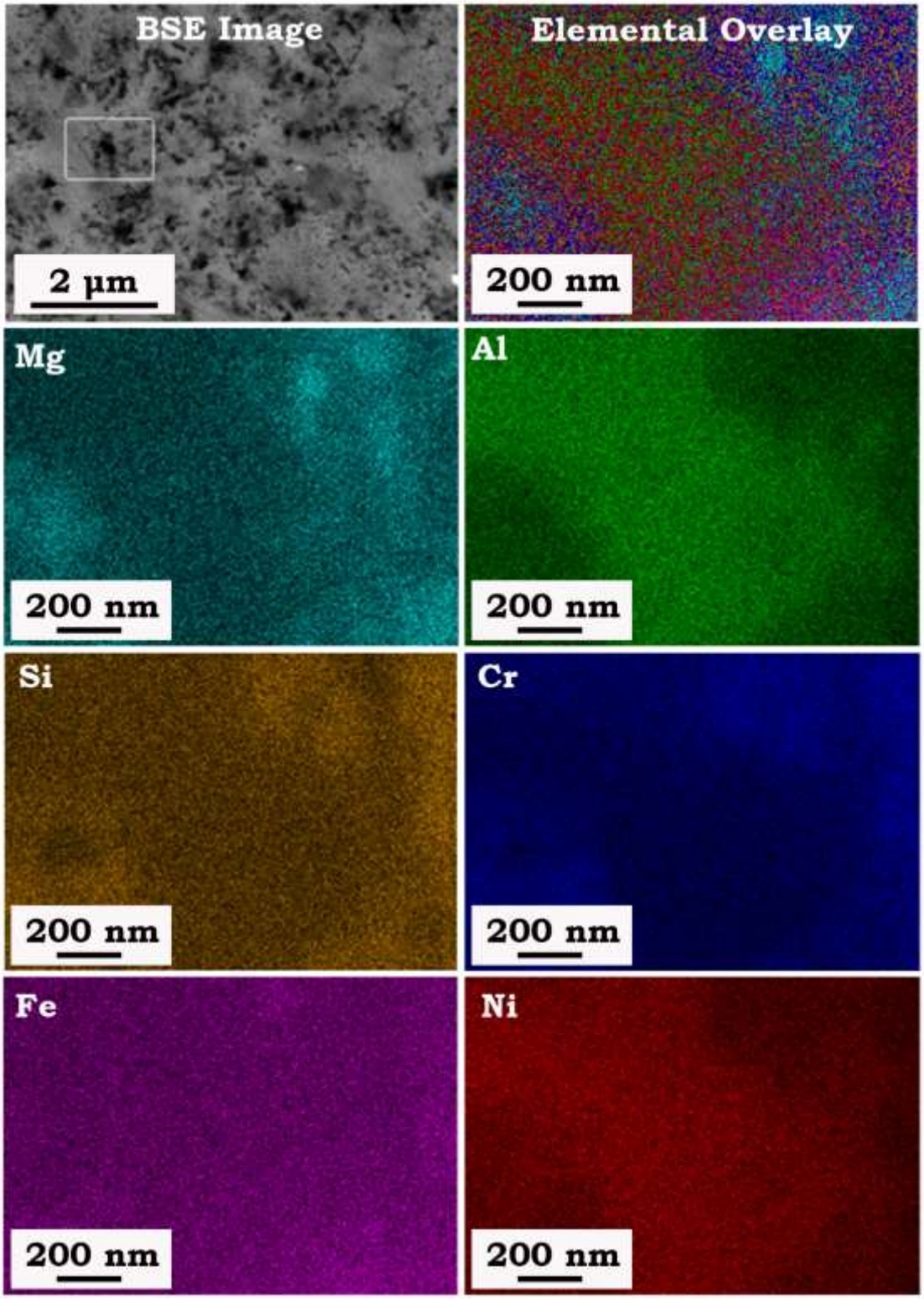

Figure 4.10: SEM – EDS elemental mapping showing distribution of elements in spark plasma sintered MgAlSiCrFeNi HEA.

4.5 Mechanical Behavior of MgAlSiCrFeNi HEA

Back-scattered images show three distinctive contrasts (i.e., bright, light grey, and dark grey) in the SEM micrograph in (Figure 4.9), which may be correlated to the XRD of the SPSed sample, as shown in Figure 4.8. The BSE-SEM micrograph used for full area scan and EDS point analysis is shown in Figures 4.9 (c) and (d), respectively. The bright contrast has a composition close to that of the equiatomic BCC phase formed after 60 h MA. The dark grey phase has a composition near to the B2-type phase, and light grey contrast was rich in Cr-Si, corresponding to the Cr_5Si_3 silicide phase. The elemental composition of the sintered samples and the points marked in Figure 4.9 (d) are mentioned in Table 4.3. Figure 4.10 represents the distribution of elements in SPSed LDHEA at 800 ℃ (1073 K). The Ni and Al-rich area may be seen from the SEM-EDS mapping. However, the Fe seems to be uniformly distributed in the entire area used for scanning. This lends support to the fact that the B2 type phase observed in the XRD (Figure 4.8) of the SPSed sample is a B2 (Ni, Al/Fe) type phase. The other elements are distributed uniformly in the area lean in Ni and Al. Hence it further strengthens the claim for two significant phases in SPSed LDHEA, i.e., BCC and B2 type phase. The density and mechanical properties of the SPSed LDHEA are mentioned in Table 4.4. It can be seen from Table 4.4 that the SPSed sample is having a density of ~99.40% and have almost no porosity, also observed in Figure 4.9.

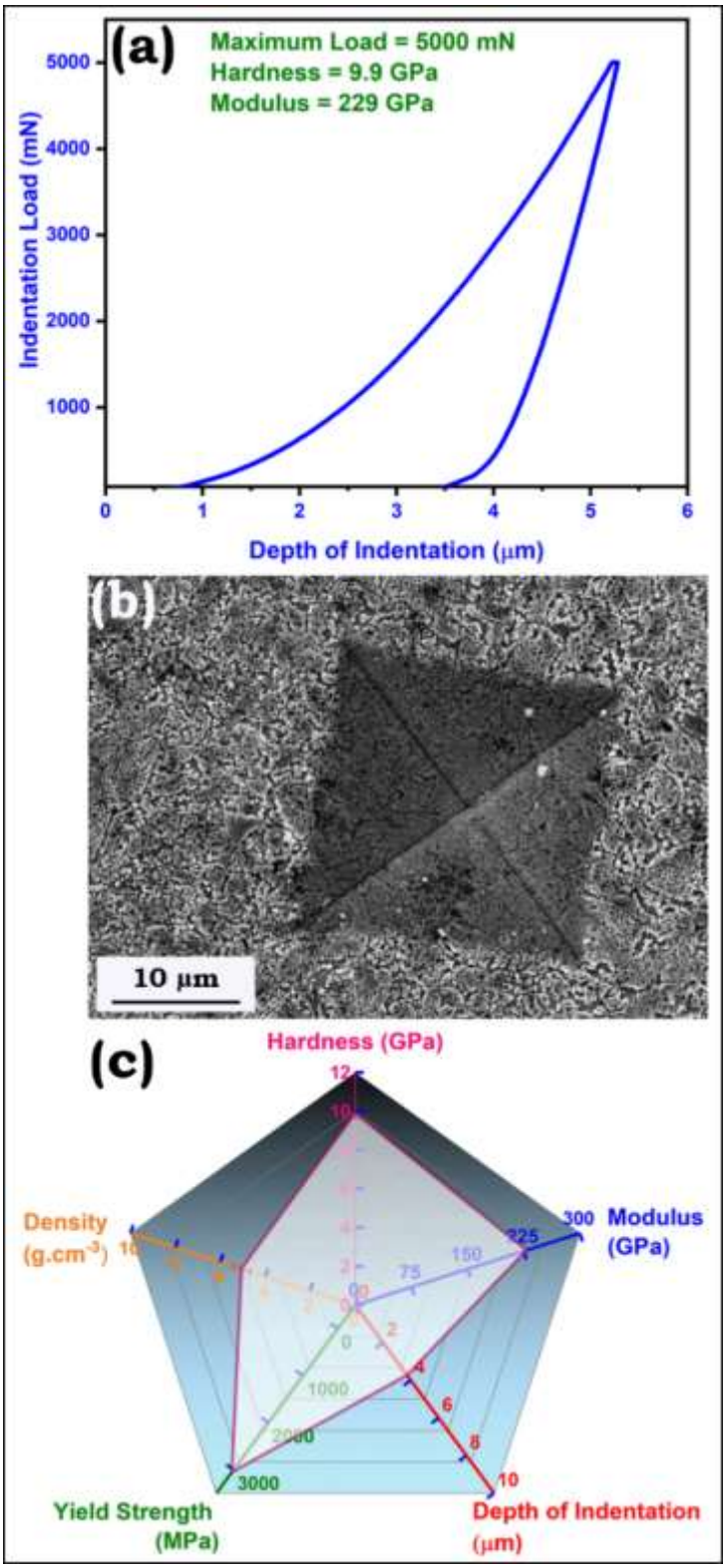

Figure 4.11: (a) Plot showing indentation load vs depth of indentation; (b) SEM micrograph showing the indentation mark at a load of 5000 mN; (c) radar diagram for mechanical property of MgAlSiCrFeNi LDHEA SPSed at 800 ℃ (1073K) for 15 min.

Table 4.3. Elemental composition of MgAlSiCrFeNi HEA SPSed sample.

Sample designation	SPS Temperature (℃)	Scan area	Elemental composition (at%)					
			Mg	Al	Si	Cr	Fe	Ni
MgAlSiCrFeNi HEA	800 ℃ (1073 K)	Full area	17.1	18.1	16.8	16.7	17.0	14.3
		Spot-1	16.9	8.7	22.6	24.7	20.1	7.0
		Spot-2	19.8	13.0	19.3	22.1	16.9	8.8
		Spot-3	15.8	23.6	14.1	13.7	15.5	17.3

The indentation behavior of these SPSed LDHEA is shown in the Figure 4.11 (a). It can be discerned from the Figure 4.11 (a) and Table 4.4, that these LDHEA have very high hardness and modulus of elasticity of ~9.98±0.3 GPa and 229±3 GPa. It was also observed that these LDHEA have a depth of penetration of ~3.75 µm at an indentation load of 5000 mN. The estimated Yield Strength (YS) of these SPSed LDHEA was found to be ~3.32 GPa (as described in Chapter 2) as per the Tabor's equation used elsewhere for these kind of HEAs [130,144]. Furthermore, it was also evident from the SEM micrograph of Figure 4.11 (b) that no indentation cracks were observed at a relatively high load of 5000 mN. The radar diagram shown in the Figure 4.11 (c) represents the various physical and mechanical properties of the SPSed LDHEA. These LDHEA have an experimental density of ~5.06 $g.cm^{-3,}$ close to many lightweight metals like Ti.

4.6 Discussion

In contrast to conventional alloys, the formation of solid solution phases in HEAs is counterintuitive to the principles of physical metallurgy. In conventional alloys one can

expect the solid solution phases at the terminal point not in the central part of the phase diagrams. The reasons of forming simple solid solution phases in HEAs have been basically explained on the basis of the high entropy effect. High entropy effect will extend the solubility limits of solid solutions to form at higher concentrations.

Table 4.4. Density and mechanical properties of SPSed MgAlSiCrFeNi LDHEA.

Sample	SPS (Temp.)	Density			Mechanical Properties		
		Theoretical Density ($g.cm^{-3}$)	Experimental Density ($g.cm^{-3}$)	Relative Density (%)	Hardness (GPa)	Modulus (GPa)	Estimated Yield Strength (GPa)
MgAlSiCrFeNi	800 ℃	5.09	5.06	99.40	9.98 ± 0.3	229 ± 3	3.32

In the present investigation, the systematic effect of parametric approach was followed to understand the phase evolutions. Thermodynamic parameters, namely enthalpy of mixing, entropy of mixing, atomic size difference, valence electron concentration and the electronegativity difference ($\Delta\chi$) were calculated. The various physical parameters used for calculating these parameters are listed in Table 4.5. The mixing enthalpy of MgAlSiCrFeNi HEA was computed using the regular solution model [35] which turn out to be – 19.33 kJ/mol. Miedema [145,146] approach was utilized to calculate the binary mixing enthalpy and values are reported in Table 4.6. The entropy of mixing as per Boltzmann's hypothesis [147] to be 14.87 J/mol.-K (Table 4.6). Atomic size difference parameter, 'δ' advocated by Zhang et al. [147] is around 11%. As per the rule for prediction of solid-solution formation in multi-component systems, the calculated values of mixing enthalpy and entropy should lie in the range of -22 to 7 kJ/mol and 11 to 19.5 J/mol.-K, respectively, as well as the atomic size parameter should be less than 8.5% [148].

Table 4.5. Physical data of constituent elements in MgAlSiCrFeNi HEA [20, 21].

Elements	**Mg**	**Al**	**Si**	**Cr**	**Fe**	**Ni**
Atomic radius (Å)	1.62	1.438	1.18	1.249	1.241	1.246
Crystal structure	HCP	FCC	DC	BCC	BCC	FCC
Melting point (°C)	650	660	1410	1863	1538	1455
Self-diffusion coefficient (m^2/s)	10^{-13}	10^{-19}	10^{-62}	10^{-41}	10^{-31}	10^{-37}

However, in the present alloy system, the parameters corresponding to the enthalpy of mixing and entropy of mixing lie within the range prescribed in the literature. However, the atomic radius difference is greater than 8.5%, which is the maximum limit for solid solution formation. Another parameter 'Ω' [147] representing the ratio between entropy and enthalpy and valence electron concentration (VEC) [147] are found to be 1.84 and 5.5 respectively for the investigated alloy. Zhang et al. [35] had proposed solid solution formation in HEA for $\Omega \geq 1$; on the contrary, $\Omega < 1$ favors the formation of intermetallic phases in a multicomponent alloys. The VEC <6.87 favors the formation of the BCC phase, while VEC>8.0 favors the FCC phase [147]. In the present investigated alloy, $\Omega > 1$, and VEC < 6.87 supporting the claim for forming the BCC phase.

The systematic observation of phase formation with milling time can be represented as follows:

0 h Mg+Al+Si+Cr+Fe+Ni (Mixed powders)

1 h Mg + Al + Si + Cr + Fe+Ni (all elements present)

10 h Mg (disappears) + Al (weak peaks disappear) + Si + Cr + Fe+ Ni

20 h Al (disappears) +Ni (minor peak disappear) + Si + (Fe + Cr)(asymmetric peak)

30 h BCC phase + Si (minor peak disappear)

40 h BCC phase (nanocrystalline) + Si (minor amount; (110) & (220) peak)

50 h BCC phase (nanocrystalline) + Si (minor amount; (110) & (220) peak)

60 h BCC phase (nanocrystalline) + Si (minor amount; (110) & (220) peak)

Single-phase BCC alloy and a minor amount of retained Si (~3 at%) were obtained after 60 h of MA for MgAlSiCrFeNi LDHEA. Chen et al. [149] have correlated the alloying rate with the melting temperature of individual element incorporated in LDHEA. The bond strength may be expected high from the high melting point of individual alloying elements. Therefore, it can be assumed that elements having a high melting point many have a lower alloying rate during mechanical alloying. Maulik et al. [139] have argued the sequence of phase formation based on bond strength as a melting temperature, atomic size, and self-diffusion coefficient, which are mentioned in Table 4.4. In spite of having a lower melting temperature than Fe and Cr, Si was unable to completely dissolved even after milling of 60h. The self-diffusion co-efficient (D) of alloying elements of MgAlSiCrFeNi LDHEA is reported in Table 4.5. In the present study it was observed that the sequence of dissolution of elements in the solid solution was also dependent on the self-diffusion co-efficient ($D(Mg) < D(Al) < D(Fe) < D(Ni) < D(Cr) < D(Si)$).

In the previous chapter, we have established the influence of self-diffusion coefficient on the alloy formation during mechanical alloying in MgAlSiCrFe. Therefore, the lower diffusion rate of Si may be one of the primary reasons for its slow diffusion and subsequent retention. This solid solution has been formed most probably due to the high entropy effect as all the alloying elements are maintained in equiatomic proportions. From the lattice parameter value of the BCC phase, it may be inferred that host lattice for this alloy system is close to α-Fe.

Table 4.6. Enthalpy of mixing (kJ/mol) of binary elements in MgAlSiCrFeNi HEA by semi-emperical Miedema's approach [14].

Elements	Mg	Al	Si	Cr	Fe	Ni
Mg	-	-2	-26	24	18	-4
Al	-2	-	-10	-11	-11	-22
Si	-26	-2	-	-37	-35	-40
Cr	24	-10	-37	-	-1	-7
Fe	18	-11	-35	-1	-	-2
Ni	-4	-22	-40	-7	-2	-

While heating the powder samples over different temperatures, exothermic heat events were observed. This implies that the milled alloy is metastable, and it resulted in several phases upon annealing. It can be said that B2 phase might be a ordered version of the parent BCC phase formed due to solute rejection [139]. For the MgAlSiCrFeNi system, the parent BCC phase is stable up to 434 ℃. At 500 °C, the emergence of a high-intensity FCC phase and parent BCC phase and a minor B2 phase was observed. The MgAlSiCrFeNi HEA powder was established to be thermally stable upto 423 ℃ (712 K).

The sequence of phase formation during annealing is as follows:

	Major Phases		**Minor Phases**
R.T	BCC	+	Si
300 ℃	BCC	+	B2 + Si
400 ℃	BCC	+	B2 + Mg_2Si + Si
500 ℃	BCC	+	B2 + FCC1 + Mg_2Si + Si
600 ℃	BCC	+	B2 + FCC1 + Mg_2Si + $Al_{13}Fe_4$
700 ℃	BCC	+	B2 + $Al_{13}Fe_4$+ FCC1 + FCC2 + Mg_2Si + Cr_5Si_3

800 ℃ BCC + B2 + $Al_{13}Fe_4$+ FCC2 + Cr_5Si_3

The phase fractions of annealed and sintered samples at 800℃ can be summarized as-

Phases	**Phase fraction (%)**	
	Annealed	SPSed
BCC/B2	64.56	61.90
Cr_5Si_3	23.79	19.99
FCC2	10.75	9.06
$Al_{13}Fe_4$	0.90	9.05

It could be observed that in both the fraction of the BCC/B2 phase is major compared to the other intermetallic phases. In the present investigation, the Ni addition stabilizes the B2 type phase formed at 800 ℃, on the contrary to the experimental finding on MgAlSiCrFe LDHEA (Chapter 3). They have reported the formation of $Al_{13}Fe_4$ as a major phase along with parent BCC and B2 phases. The formation of intermetallic phases enhances the phase stability of these alloys at higher temperature. Thus while designing HEAs it is essential to control the formation of the intermetallic phase. In our alloy systems, intermetallics are present in a small amount along with the major BCC phase and B2 phase. The appearance of Cr_5Si_3 can be ascribed to the high negative enthalpy of the formation of Cr-Si. The high hardness in these LDHEA (Table 4.4) may be attributed to the formation of various intermetallics and silicides along with the parent BCC phase. Similar observation was also made by Jain et al. [150] for high entropy steel fabricated by mechanical alloying and spark plasma sintering.

Table 4.7. Calculated thermodynamic and other parameter of MgAlSiCrFeNi HEA.

ΔH_{mix} $\left(kJ/mol\right)$	ΔS_{conf} $\left(\frac{JK^{-1}}{mol}\right)$	T_m (K)	Ω	δ (%)	VEC	Δχ
-19.84	14.87	1535	1.84	11	5.5	0.212

In similar line with the present investigation, Shivam et al. [151] has recently reported the formation of B2-type (NiAl) phase in a BCC high entropy alloy matrix. These nano-precipitates of B2-type phase enhance the mechanical properties of the non-equiatomic FeCrNiAlCo HEA to a greater extent. This appreciable value of hardness and modulus envisages its potential usage for structural application.

4.7 Conclusions

The following conclusions can be drawn from the present chapter:

1. An equiatomic MgAlSiCrFeNi HEA having a major solid solution phase of BCC structure (a= 0.2876 ± 0.003 nm) was successfully synthesized through mechanical alloying. A minor amount of Si (~3 %) was found to be undissolved.
2. Nanocrystalline nature (a size of ~15 nm) of 60 h milled MgAlSiCrFeNi LDHEA powder with a BCC phase and small amount of Si was confirmed by TEM. The alloy is established to be thermally stable up to a temperature of ~400 ℃ (673 K). The annealing treatment above 400 ℃ (673 K) led to the evolution of a significant BCC phase and B2 along with a minor amount of other phases i.e., $Al_{13}Fe_4$, FCC phase, Cr_5Si_3, Mg_2Si.

3. The atomic size difference factor (~11%), positive mixing enthalpy of binary Mg-Cr, Mg-Fe, and high negative enthalpy of mixing among Mg-Si, Cr-Si, Fe-Si, Al-Ni, and Ni-Si are unfavorable for the stability of a single-phase solid solution. Hence it leads to a number of several phases after annealing treatment. Thus, alloy design for HEAs a challenging task for developing a single-phase solid solution in the multicomponent alloy system.
4. The SPSed LDHEA also exhibits a similar phase as observed for the annealed sample at 800 ℃ (1073 K) with the density of 5.06 $g.cm^{-3}$. The SPSed LDHEA sample exhibits very high value of hardness and modulus of elasticity of ~9.98 and 229 GPa respectively due to co-existence of B2, $Al_{13}Fe_4$ phase, silicides along with parent BCC phase in the SPSed LDHEA.